Prediction of stochastic limit cycle oscillations using an adaptive Polynomial Chaos method

Josselin Le Meitour[1]
Didier Lucor[2,3]
Jean-Camille Chassaing[2,3]

(Received: Jul 30, 2009. Revised: Feb 8, 2010. Accepted: Mar 16, 2010)

Abstract
In this paper a non-intrusive adaptive stochastic spectral projection method is employed to predict limit-cycle oscillations (LCO) of an elastically mounted airfoil with random structural properties. Due to the nonlinear dynamics of the aeroelastic system, the use of a local stochastic representation based on a partition of the parametric space is more appropriate than a global approximation. Here, the stochastic response of the airfoil due to several uncertain structural parameters is expanded on a multi-element generalized Polynomial Chaos basis. The parametric space is discretized and a cubature grid is prescribed on each element of the partition. A particular attention is paid to the computation of the stochastic supercritical bifurcation obtained when a hardening spring is considered as the nonlinear restoring pitching force. Numerical results show how the probability density function of the peak pitch response, computed for both supercritical and subcritical branches, is affected by independent multiple input random parameters with bounded distributions. The efficiency and robustness of the multi-element approach is investigated by means of analysis of h/p convergence and comparison with Monte-Carlo simulations and various stochastic bifurcation behaviors are investigated in details.

1. Introduction

The prediction of the flutter onset speed is of great importance in the field of aeroelasticity. The corresponding loss of dynamic stability, which results in unbounded vibrations of the structure, may lead to the failure of aircraft components [7, 5]. When nonlinearities are present into the structural or aerodynamic operator, the growth in the amplitude of the response is stabilized to limit cycle oscillations (LCO) [15, 16]. These oscillations can be seen as the consequence of the bifurcation from a stable solution to an oscillatory behavior of the nonlinear dynamic system. Depending of the nature of the nonlinear restoring forces, one can expect to get both supercritical (small amplitude LCO) or subcritical (large amplitude LCO) when transitioning through the Hopf bifurcation point [15, 16, 1, 23]. The former can lead to an excessive fatigue of the structure while the latter results in destructive flutter. The influence of the structural parameters on the deterministic LCO response of a pitch-and-plunge airfoil has been widely studied for various types of structural nonlinearities (see [15] for an extensive review).

Because LCO are inherently sensitive to small variations of both the structural parameters and initial conditions [15, 23], stochastic methodologies devoted to the propagation of uncertainties are promising candidates to obtain more insights in the physical flutter mechanism and LCO [1, 25] with affordable computational requirements.

Although accurate uncertainty quantification can be performed for steady stochastic airfoil flows using stochastic spectral methods based on generalized Polynomial Chaos (gPC) expansions [32, 10, 4], the prediction of strongly nonlinear problems such as stochastic limit-cycle oscillations requires the use of more advanced stochastic methods. This is because global gPC approaches suffer from

[1] Ecole Normale Supérieure de Cachan, 61 Av. du Président Wilson, 94230 Cachan, France
[2] UPMC, Univ Paris 6, UMR 7190, Institut Jean Le Rond d'Alembert, F-75005 Paris, France
[3] CNRS, UMR 7190, Institut Jean Le Rond d'Alembert, F-75005 Paris, France

doi:10.3293/asdj.2010.4

lack of robustness in the modeling of stochastic oscillating systems involving long-term integration and/or discontinuities in the random space [33, 28, 1, 40].

Millman el al.[24] developed a stochastic projection method based on Fourier Chaos expansion to compute the probability density functions (pdf) of the peak LCO for both subcritical and supercritical branches of the bifurcation diagram in the case of Gaussian distributions of the cubic spring coefficient in pitch and the initial pitch angle.
This problem was also studied using non-intrusive B-spline stochastic projections [23], or Wiener-Haar and Wiener-Hermite expansions [1]. Stochastic LCO and bifurcation diagram were explored by Wu et al.[41] by means of bounded random variables with λ-pdf. The Gegenbauer polynomials were employed, as a family of orthogonal basis for the function expansions, to compute the Hopf-bifurcation point, the flutter speed and the angular frequency of the stochastic system.
Witteveen et al.[40] proposed a probabilistic collocation method for limit cycle oscillations (PCLCO) for the study of period-1 limit cycle oscillations with one main frequency subject to randomness. This method, which is based on the use of non-intrusive probabilistic collocation in conjunction with a time-independent parametrization of the periodic response of the deterministic samples, was found to be efficient for resolving the long-term stochastic effect of random parameters. This approach was initially limited to period-1 oscillations of stochastic simulations with a single random parameter. In Ref. [37] Witteveen and Bijl developed a time-independent unsteady stochastic finite elements (UASFEi-ti) method based on an extension of the stochastic finite element (ASFE) approach with time-independent parametrization. Note that in Ref. [36], the unsteady stochastic finite elements method based on interpolation with constant phase (UASFE-cp) was found to be an interesting alternative to the UASFE-ti formulation because it eliminates the parametrization error, resolves time-dependent functionals and captures transient behavior of the samples. The discussion about the total variation diminishing (TVD) properties in probability space of the UASFE approach is presented in Ref. [39]. Recently, Witteveen and Bijl [38] have successfully investigated the higher period stochastic bifurcation of a nonlinear airfoil model. In particular, they have found that both randomness in the cubic restoring coefficient in pitch and the initial pitch angle induce large effects at the second stochastic bifurcation point.

A different approach was considered by Wan and Karniadakis [33] who developed a multi-element (ME) intrusive approach based on gPC expansions to maintain the accuracy of the gPC for stochastic problems involving both long-term integration and discontinuities in random space. The need for extensive computational resources was limited by the use of criterion to perform the the random space partition. The h/p-type convergence of the ME-gPC for a 2D stochastic is presented in the case of a convection-diffusion problem for *uniform* random inputs and Legendre-Chaos. The generalization of the ME-gPC to arbitrary random variables is presented in Ref. [34].

The scope of the present study is to assess if the non-intrusive ME-gPC formulation is able to correctly predict the stochastic response of aeroelastic systems in the presence of discontinuities in the random space; compared to a Stochastic Finite Elements method, which implies a partition of the random space but is limited to a fixed order expansion (e.g. linear or quadratic) [37, 36], our method is *adaptive* in h (typical size of the element) and allows the use of high p (typical order of the the local gPC expansion). The mathematical formulation of the multi-element gPC method is briefly presented in section 2. Then the numerical solutions of nonlinear aeroelastic governing equations are described in section 3. The numerical ME-gPC results are discussed in details in section 4.

2. Uncertainty quantification numerical approach

2..1 Generalized Polynomial Chaos framework

The generalized Polynomial Chaos (gPC) method is a non-statistical method used to solve stochastic differential (SDE) and stochastic partial differential equations (SPDE) and has been used for numerous applications. It is a spectral representation of a random process in terms of orthogonal basis functions; the spatial and temporal evolutions of the basis coefficients providing quantitative estimates of the modeled random process solution.

2..1.1 Non-intrusive formulation

The original polynomial chaos was first proposed by N. Wiener and re-introduced more recently by Ghanem [8]. It employs the Hermite polynomials in terms of Gaussian random variables as the trial basis to expand stochastic processes in the random space. According to the theorem by Cameron and Martin [3] such expansion converges for any second-order processes in the L_2 sense. More specifically, they have proved that any nonlinear functional of a brownian motion can be represented with mean-square convergence as a Wiener-Hermite series. The importance of this theorem is that it extends obvious results from finite-dimensional approximations (where various polynomials are complete with respect to their respective measures), to an infinite-dimensional context (brownian motion instead of a finite set of random variables). Even if there is no parallel result for general measures (except for the Poisson and binomial measure [29]), Xiu et. al [42] have proposed a generalization of the original Hermite-chaos. Their representation employs different types of orthogonal polynomials from the Askey family [29] and can deal efficiently with non-Gaussian random inputs in many cases, e.g. [21, 35, 22].

Let $(\Omega, \mathcal{F}, P)$ be a probability space. Let $\boldsymbol{\xi} = (\xi_1, \ldots, \xi_d)$ be a $\mathbb{R}^d$-valued continuous random variable, where $d \in \mathbb{N}$. Any second-order random process $u(\omega)$ can be expressed by gPC as

$$u(\omega) = \sum_{i=0}^{M} \hat{u}_i \Phi_i(\boldsymbol{\xi}(\omega)) \tag{1}$$

where ω is the random event and $\Phi_i(\boldsymbol{\xi}(\omega))$ denotes the gPC basis in terms of the random variable $\boldsymbol{\xi}$. The total number of modes M is determined by the dimension d of $\boldsymbol{\xi}$ and the order of the local gPC expansion P

$$M + 1 = \frac{(P+d)!}{P!d!} \tag{2}$$

The family $\{\Phi_i\}$ is an orthogonal basis in $L_2(\Omega, \mathcal{F}, P)$ with orthogonality relation

$$\mathbb{E}[\Phi_i \Phi_j] = \mathbb{E}[\Phi_i^2]\delta_{ij} \tag{3}$$

where $\mathbb{E}$ denotes the expectation with respect to the probability measure $dP(\omega) = f(\xi(\omega))d\omega$. Here, we focus on a non-intrusive approach where the gPC coefficients are obtained from Galerkin projection of the stochastic solution directly onto each member of the orthogonal basis chosen to span the random space:

$$\hat{u}_i \quad = \quad \frac{\mathbb{E}(u(\boldsymbol{\xi}), \Phi_i(\boldsymbol{\xi}))}{\mathbb{E}(\Phi_i^2(\boldsymbol{\xi}))} \quad \text{for} \quad i = 0, ..., M. \tag{4}$$

In this study, the expectations are evaluated thanks to numerical cubatures with a number of points which is chosen *a priori* depending on accuracy and cost requirements. This choice will be motivated in the next section. This approach is very flexible as it does not require modifications to the existing deterministic solver.

2..1.2 Numerical quadratures

The evaluation of Eq. 4 is equivalent to computing multi-dimensional integrals over the stochastic domain. Different ways of dealing with high-dimensional integrations can be considered depending on the prevalence of accuracy versus efficiency. A convenient approximation through numerical cubature consists in replacing the integral by a finite weighted sum of the integrand values taken at some chosen points.

Among the different quadrature rules available we have chosen Gauss type quadrature formulas [9, 31] in which point locations and corresponding weights are directly based on the probability measure appearing in the expectation computation, Eq. 3. Gauss quadratures are known for their high level of polynomial exactness : i.e. a N-points rule makes it possible to integrate *exactly* polynomial functionals up to order $(2N-1)$.

In this study, we construct our cubature based on full tensor products of Gauss-Legendre one dimensional quadrature rules. This is not too costly as our number of random dimensions is small. We insist on the fact that the deterministic solver will compute/provide the solution output at those *known* quadrature points and not at randomly selected locations. The number of quadrature points to use will depend on the regularity of the function to integrate. First the *known* polynomial exactness of our cubature makes it possible to predict the number of points needed to evaluate the inner products involved in Eq. 3. Next, we increment *a posteriori* the number of grid points (if required) by carrying out a convergence analysis of the solution, e.g. Fig. 3. This is due to the (possibly) non-polynomial nature of the solution.
When the number of grid points in multi-dimensions d becomes too large, one should not use a grid based on the full tensor product of one-dimensional grids. An alternative is to use sparse quadratures which require less quadrature points. For instance, the sparse quadrature based on Smolyak algorithm [30] has the advantage of remaining accurate with a convergence rate depending weakly on the number of dimensions.

2..2 Adaptive ME-gPC formulation

It is well known that although global gPC can achieve exponential convergence for smooth problems, it may converge slowly or even fail to converge in case of discontinuities (such as strong shocks) or steep fronts in random space [28]. In the following, we closely follow the mathematical framework proposed by Wan and Karniadakis [33] to overcome these limitations. We introduce the scheme of the adaptive multi-elements generalized Polynomial Chaos (ME-gPC) method: partition of random space, construction of orthogonal polynomials and an adaptive procedure in order to deal with these problems.

2..2.1 Random space partition

The goal in the following is to represent the stochastic solution in a partitioned random space. To this end, we will have to construct a piecewise polynomial basis, orthogonal with respect to the local probability distribution. We will first define the partition space, then derive the conditional probabilities, and finally, we deal with the ME-gPC approximation.

We assume that $\boldsymbol{\xi}$ is a random variable defined on $B = \times_{i=1}^{d}[a_i, b_i]$, where a_i and b_i are finite in $\mathbb{R}$ and the components of $\boldsymbol{\xi}$ are independent identically-distributed (i.i.d.) *uniform* random variables. We define a $N-$element partition $\mathbf{D}$ of B as

$$\mathbf{D} = \begin{cases} B_k = [a_{k,1}, b_{k,1}) \times [a_{k,2}, b_{k,2}) \times \cdots \times [a_{k,d}, b_{k,d}] \\ B = \bigcup_{k=1}^{N} B_k \\ B_{k_1} \bigcap B_{k_2} = \emptyset, \text{ if } k_1 \neq k_2 \end{cases} \tag{5}$$

where $k, k_1, k_2 = 1, 2, \cdots, N$. Based on the partition $\mathbf{D}$, we define the following indicator random variables

$$I_{B_k} = \begin{cases} 1 & \text{if } \boldsymbol{\xi} \in B_k, \\ 0 & \text{otherwise.} \end{cases} \qquad k = 1, 2, \cdots, N. \tag{6}$$

Using Bayes' rule, we define a new random variable $\boldsymbol{\xi}_k : I_{B_k}^{-1}(1) \mapsto B_k$ on the probability space $(I_{B_k}^{-1}(1), \mathcal{F} \cap I_{B_k}^{-1}(1), P(\cdot | I_{B_k} = 1))$ subject to a conditional pdf

$$\hat{f}_k(\boldsymbol{\xi}_k | I_{B_k} = 1) = \frac{f(\boldsymbol{\xi}_k)}{\Pr(I_{B_k} = 1)} \tag{7}$$

in each random element B_k, where $\Pr(I_{B_k} = 1) > 0$.

Let $u(\boldsymbol{x}, t; \boldsymbol{\xi}) \in L_2(\Omega, \mathcal{F}, P)$ denote a *second-order* space-time related random field. For simplicity, we may drop $\boldsymbol{x}$ and t. To approximate a random field $u(\boldsymbol{\xi})$ using ME-gPC, we expand the random field spectrally in each element B_k, then re-construct the entire random field by the following proposition. Let $\hat{u}_k(\boldsymbol{\xi}_k)$ be the local polynomial chaos expansion in element B_k. The approximation on the entire random field can be defined as

$$u^r(\boldsymbol{\xi}) = \sum_{k=1}^{N} \hat{u}_k(\boldsymbol{\xi_k}) I_{B_k} = \sum_{k=1}^{N} \sum_{j=0}^{M} \hat{u}_{k,j} \Phi_{k,j}(\boldsymbol{\xi_k}) I_{B_k} \tag{8}$$

which converges to $u(\boldsymbol{\xi})$ in the L_2 sense, in other words,

$$\int_B (u^r(\boldsymbol{\xi}) - u(\boldsymbol{\xi}))^2 f(\boldsymbol{\xi}) \mathrm{d}\boldsymbol{\xi} \to 0, \quad \text{as } M \to \infty. \tag{9}$$

By Bayes' rule and the law of total probability, any statistics can be obtained as

$$\int_B g\left(u(\boldsymbol{\xi})\right) f(\boldsymbol{\xi}) \mathrm{d}\boldsymbol{\xi} \approx \sum_{k=1}^{N} \Pr(I_{B_k} = 1) \int_{B_k} g\left(\hat{u}_k(\boldsymbol{\xi}_k)\right) \hat{f}_k(\boldsymbol{\xi}_k | I_{B_k} = 1) \mathrm{d}\boldsymbol{\xi}_k \tag{10}$$

where $g(\cdot) \in L_1(\Omega, \mathcal{F}, P)$ is a functional of random field $u(\boldsymbol{\xi})$.

2..2.2 Local orthogonal polynomial basis

With classical gPC formulation, we usually use Legendre polynomials for the basis when we deal with uniform distributions. For the multi-element approach, one has to build orthogonal polynomials with respect to the local distribution (see Eq. 7) within the element of interest. This step can be problematic for some distributions, but becomes obvious for uniform/Legendre discretization. In this case, the local polynomials to the element remain Legendre polynomials and only a scaling is necessary to map the element to a standard element of reference.

2..2.3 Sensitivity based adaptivity

Let us define the local solution variance given by gPC representation with order P

$$\sigma_{k,p}^2 = \sum_{j=1}^{M_P} \hat{u}_{k,j}^2 \mathbb{E}[\Phi_{k,j}^2] \tag{11}$$

while the *approximate* global mean $\bar{u}$ and variance $\bar{\sigma}^2$ can be expressed as

$$\bar{u} = \sum_{k=1}^{M} \hat{u}_{k,0} \Pr(I_{B_k} = 1), \quad \bar{\sigma}^2 = \sum_{k=1}^{M} \left[\sigma_{k,p}^2 + (\hat{u}_{k,0} - \bar{u})^2\right] \Pr(I_{B_k} = 1) \tag{12}$$

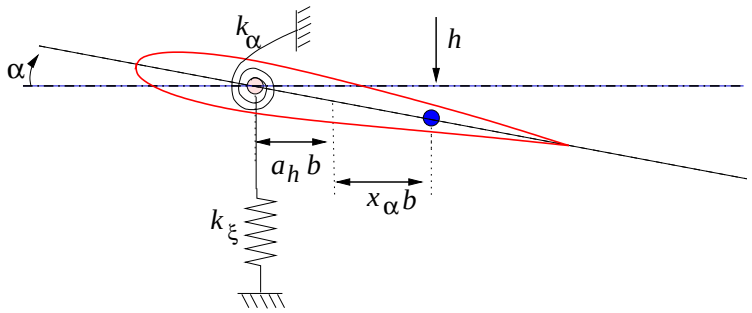

Figure 1: Two-degree-of-freedom pitch-and-plunge airfoil model

We measure the decay rate of the relative error of the representation in each element as

$$\eta_k = \frac{\sum_{i=M_{P-1}+1}^{M_P} \hat{u}_{k,i}^2 \mathbb{E}[\Phi_{k,i}^2]}{\sigma_{k,p}^2} \tag{13}$$

Based on η_k and the probability $\Pr(I_{B_k} = 1)$, we decompose the current random element, if the following criterion

$$\eta_k^\gamma \Pr(I_{B_k} = 1) \geq \theta_1, \quad 0 < \gamma < 1 \tag{14}$$

is satisfied, where γ and θ_1 are prescribed constant parameters. In order to maintain an affordable number of total elements for problems involving multiple random variables, we select the most sensitive random dimensions based on the following criterion developed by Wan and Karniadakis [33]:

$$r_i = \frac{\hat{u}_{i,P}^2 \mathbb{E}[\Phi_{i,P}^2]}{\sum_{j=M_{P-1}+1}^{M_P} \hat{u}_j^2\, \mathbb{E}[\Phi_j^2]}, \qquad i = 1, 2, \cdots, d \tag{15}$$

where we neglect the subscript k for clarity and the subscript $\cdot_{i,P}$ denotes the mode consisting only of random dimension ξ_i with polynomial order P. All random dimensions which satisfy

$$r_i \geq \theta_2 \cdot \max_{l=1,\cdots,d} r_l, \tag{16}$$

will be split into two random elements in the next step while all other random dimensions remain unchanged.

3. Deterministic aeroelastic model and solvers

In this study, we consider a typical section airfoil model subjected to a two-degree-of-freedom motion with plunge displacement of the elastic axis h and pitch angle α (about the elastic axis). The additional mechanical parameters, which are represented in Fig. 1, are the static unbalance x_α, and the non-dimensional distance between the mid-chord and the elastic axis a_h.

The coupled bending-torsion equations of motion can be written in non-dimensional form as follows [13]

$$\xi'' + x_\alpha \alpha'' + 2\zeta_\xi \frac{\bar{\omega}}{U^*} \xi' + \left(\frac{\bar{\omega}}{U^*}\right)^2 k_\xi \xi = -\frac{1}{\pi\mu} C_L(\tau) \tag{17}$$

$$\frac{x_\alpha}{r_\alpha^2} \xi'' + \alpha'' + 2\frac{\zeta_\alpha}{U^*} \alpha' + \left(\frac{1}{U^*}\right)^2 k(\alpha) = \frac{2}{\pi\mu r_\alpha^2} C_M(\tau) \tag{18}$$

where $\xi = h/b$ denotes the nondimensional displacement of the elastic axis with half-chord b, r_α is the radius of giration about the elastic axis, μ represents the

mass ratio, the viscous damping coefficients in pitch and plunge are ζ_α and ζ_ξ respectively, and $\bar{\omega} = \omega_h/\omega_\alpha$ is the frequency ratio computed from the uncoupled plunging ω_h and ω_α frequencies of the undamped motion. The nondimensional velocity is determined as $U^* = U/(b\omega_\alpha)$ and the $'$ refers to differientiation with respect to the nondimensional time $\tau = Ut/b$.

The aerodynamic operator is described through the lift and the pitching moment coefficients $C_L(\tau)$ and $C_M(\tau)$. For an incompressible flow over an oscillating airfoil undergoing arbitrary small-amplitude motions, we use the unsteady linear aerodynamic model given by Fung [7]

$$\begin{aligned} C_L(\tau) &= \pi(\xi'' - a_h\alpha'' + \alpha') + 2\pi\{\alpha(0) + \xi'(0) + [\frac{1}{2} - a_h]\alpha'(0)\}\phi(\tau) \quad (19) \\ &\quad +2\pi\int_0^\tau \phi(\tau-\sigma)[\alpha'(\sigma) + \xi''(\sigma) + (\frac{1}{2} - a_h)\alpha''(\sigma)]d\sigma \\ C_M(\tau) &= \pi(\frac{1}{2} + a_h)\{\alpha(0) + \xi'(0) + (\frac{1}{2} - a_h)\alpha'(0)\}\phi(\tau) \\ &\quad +\pi(\frac{1}{2} + a_h)\int_0^\tau \phi(\tau-\sigma)\{\alpha'(\sigma) + \xi''(\sigma) + (\frac{1}{2} - a_h)\alpha''(\sigma)\}d\sigma \\ &\quad +\frac{\pi}{2}a_h(\xi'' - a_h\alpha'') - \frac{\pi}{2}(\frac{1}{2} - a_h)\alpha' - \frac{\pi}{16}\alpha'' \quad (20) \end{aligned}$$

The Wagner function $\phi(\tau)$ is computed using the two states approximation from R.T. Jones [11]

$$\phi(\tau) = 1 - \Psi_1 e^{-\varepsilon_1\tau} - \Psi_2 e^{-\varepsilon_2\tau} \quad (21)$$

with $\Psi_1 = 0.165$, $\varepsilon_1 = 0.0455$, $\Psi_2 = 0.335$ and $\varepsilon_2 = 0.3$.

Finally, the highly nonlinear behavior of the airfoil motion is obtained by modeling the pitching restoring forces $k(\alpha)$ such that [24]

$$k(\alpha) = k_{\alpha_1}\alpha + k_{\alpha_3}\alpha^3 + k_{\alpha_5}\alpha^5 \quad (22)$$

where the stiffness coefficients k_{α_i} $(i = 1, 3, 5)$ can be considered either as deterministic parameter or random variables.

The governing equations of motion result in a set a two second-order differential equations whose coefficients are functions of the system parameters. See, for example, Lee et al.[15] for the expression of these coefficients in the case where $k_\xi = k_{\alpha_1} = 1$. As far as the time-domain formulation of the problem is concerned, the governing equations of motion are re-arranged in a set of eight first-order ordinary differential equations [15] which is solved using an explicit fourth-order Runge-kutta time-integration scheme [13, 26, 18, 41, 40, 27].

For oscillatory motions dominated by the first harmonic, we compute the LCO amplitude using the 1st order harmonic balance procedure developed by Lee et al.[14]. Toward this end, the governing equations are formulated in frequency-domain by means of the following decomposition [14]

$$\alpha(\tau) = a_1\sin(\omega\tau), \qquad \xi(\tau) = e_1\sin(\omega\tau) + f_1\cos(\omega\tau) \quad (23)$$

Inserting the previous relations (Eqs. 23) in the governing equations (Eqs 17, 18) and collecting the coefficients of $\sin(\omega\tau)$ and $\cos(\omega\tau)$ gives a nonlinear system of fourth equations of a_1, e_1, f_1 and ω. For the particular case where $a_h = -0.5$ and $k_{\alpha_5} = 0$, Lee et al.[14] derived a sixth-degree polynomial equation for the frequency parameter ω. Then the expression of the amplitudes of the plunge and pitch motions can be computed analytically. Here, the harmonic balance solver of Ref. [13] was slightly modified in order to account for parametric studies of the linear spring coefficients k_ξ and k_{α_1}. The use of more advanced frequency-domain approaches such as incremental harmonic balance methods [12, 2] and high-order or high-dimensional harmonic balance methods [17, 18, 20, 19] is beyond the scope of the present study.

Both the Runge-Kutta and the harmonic balance solvers are coupled in this work with the ME-gPC method but the latter will be preferred for simulations with period-1 LCO and hardening-spring nonlinearity because of its computational efficiency and accuracy in the prediction of LCO amplitudes.

4. Uncertainty quantifications of LCO

In this study, the quantity of interest is the peak pitch amplitude α_A. However, similar stochastic analysis may be conducted on the LCO frequencies or on the peak plunge amplitude since the ME-gPC formulation is applicable to any outputs delivered by the deterministic solver.

Unless otherwise specified , the values of the deterministic parameters used for the numerical results are taken as [13]

$$\begin{aligned} r_\alpha = 0.5, \quad x_\alpha = 0.25, \quad \bar{\omega} = 0.2, \quad \mu = 100 \\ a_h = -0.5, \quad \zeta_\alpha = 0, \quad \zeta_\xi = 0 \quad k_{\alpha_5} = 0 \end{aligned} \tag{24}$$

The coefficients describing the nonlinear torsional stiffness are considered as random parameters with bounded distributions. Stochastic results are analysed by means of the response surface, statistical moments and pdf of the peak pitch amplitude α_A since nonlinearities were introduced in the torsional restoring forces only.

Millman et al. in [23, 24] have studied the influence of uncertainties associated to the initial pitch angle $\alpha(0)$ and cubic torsional stiffness term k_{α_3} onto the stochastic LCO. In this study, deeper investigations are proposed by means of the analysis of several stochastic configurations: Case-1 is devoted to the study of cubic torsional stiffness randomness in the presence of supercritical bifurcations. Then, the effect of combined uncertainties in both the linear k_{α_1} and cubic k_{α_3} torsional stiffness terms is investigated in case-2. The ability of dealing with realizations ranging from the subcritical to the supercrital branches is demonstrated in case-3. Finally, case-4 is considered to perform a sensitivity study of the subcritical peak LCO to combined randomness in linear torsional stiffness and the initial pitch angle.

4..1 *Case-1: effect of randomness of the cubic torsional stiffness term*

In order to verify the correct implementation of the coupling procedure between gPC and the deterministic harmonic balance aeroelastic solver, we consider first the case of a single uncertainty in the cubic torsional stiffness k_{α_3}. The input random variable is then expressed in standard form

$$k_{\alpha_3} \quad = \quad \bar{k}_{\alpha_3} + \sigma_{k_{\alpha_3}} \xi_1 \tag{24}$$

with $\bar{k}_{\alpha_3} = 3$ and $\sigma_{k_{\alpha_3}} = 0.75$ and ξ_1 is a random variable following a uniform distribution with zero mean and unit variance. It is well known that the influence of k_{α_3} does not affect the onset of the flutter boundary [15, 41]. Therefore, the use of a multi-element approach is not necessary in this case. The stochastic simulation was performed using a 8th order gPC expansion. The harmonic balance solver was considered in order to prevent the deterministic errors from masking the global error of the stochastic gPC representation.

Fig. 2a depicts the pdf isocontours of the pitch amplitude α_A for nondimensional speeds ranging from $U^* = 6.1$ up to $U^* = 7$. Here, we use an $8th$ order gPC expansion to evaluate the pdfs. The pdf contours are normalized at each streamwise location such that the maximum probability density is always unity. This is done because we are more interested by the distribution of the strongest gradients and most probable solutions than by the actual probability magnitudes. Keeping in mind that k_{α_1} was modeled using a *uniform* random distribution, it is interesting to note that the pdf of α_A is not uniform. Furthermore, the maximum values of the pdf are always obtained for the lower values of

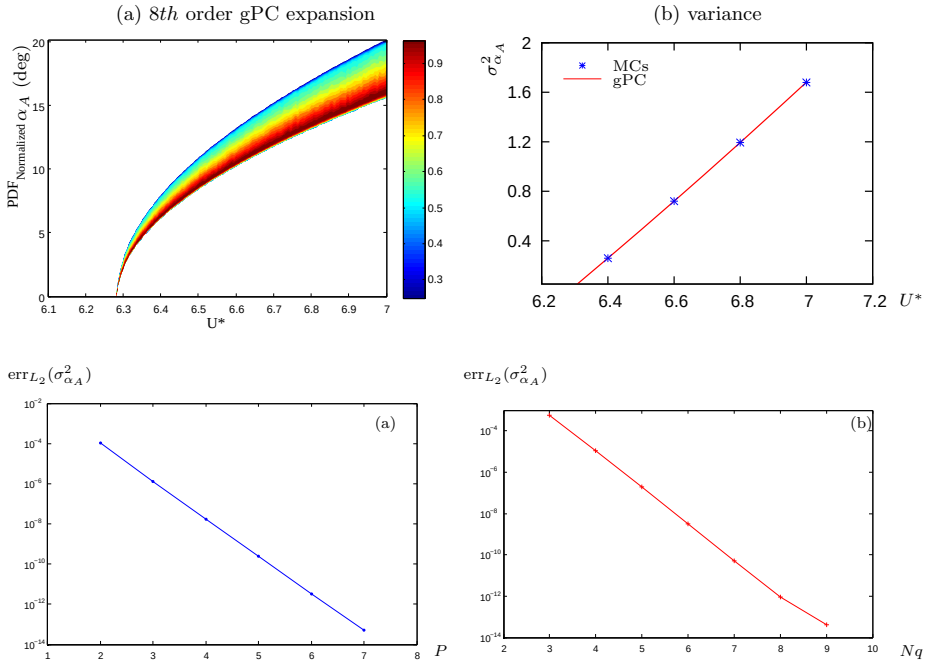

Figure 2: Case-1: (a) gPC pdf isocontours of α_A due to uncertain k_{α_3} and (b) variance comparison with Monte-Carlo simulations with $N_{MC} = 10^6$ samples

Figure 3: Case-1: gPC convergence rate of the variance of σ_{α_A} with respect to the polynomial order P (a) and the number of cubature points N_q per direction (b)

the possible range of solutions (corresponding to the red color in the pdf). One may also remark on Fig. 2a that the spread of the stochastic solution increases with U^*.

Fig. 2b presents a comparison of the solution variance of the peak pitch angle $\sigma^2_{\alpha_A}$ computed using gPC and Monte-Carlo simulations with $N_{MC} = 10^6$ samples. The agreement is excellent for the whole bifurcation diagram ($U^* \in [6.4, 7]$) and the linear growth of $\sigma^2_{\alpha_A}$ with the bifurcation parameter U^* is clearly observed.

Fig. 3 shows the convergence of the solution variance of α_A both with respect to the polynomial order P and the number of quadrature points N_q per random direction.

The reference solution is taken to be the most resolved gPC results obtained using $P = 8$. The straight lines (here, relative error in variance) in semi-log vertical axis plots confirm the spectral (exponential) P-type convergence of the representation for this type of smooth response.

4..2 *Case-2: Influence of combined uncertainties in the linear and cubic torsional stiffness terms*

Next, a stochastic problem with two random dimensions is investigated by means of combined uncertainties in the linear and cubic torsional stiffness terms with $\bar{k}_{\alpha_1} = 1$ and $\sigma_{k_{\alpha_1}} = 0.1$. The mean value and the standard deviation of k_{α_3} remains unchanged ($\bar{k}_{\alpha_3} = 3$, $\sigma_{k_{\alpha_3}} = 0.75$).

The response surfaces displayed on Fig. 4 are constructed using gPC with $P = 15$ and ME-gPC with $P = 3$. The value of $U^* = 6.34$ was selected such that the corresponding response surface presents a discontinuity in the random space driven by k_{α_1}. Although gPC is able to predict the global behavior of the response (Fig. 4a), it fails in accurately capturing the sudden change in the response, even when a high polynomial order is employed ($P = 15$). Note also that the response surface presents non-physical oscillations around the stationary state obtained for $k_{\alpha_1} = 1$ up to $k_{\alpha_1} = 1.1$. On the other hand, the multi-element solver based on a low gPC expansion ($P = 3$) raises immediately these drawbacks by successively refining the random elements around the discontinuity located at $k_{\alpha_1} = 0.98$ (Fig. 4b).

The first two statistical moments of the peak amplitude of α_A present a good

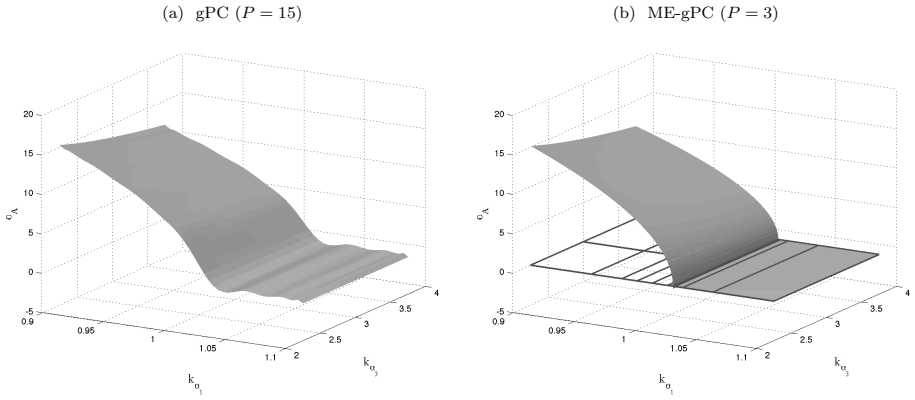

Figure 4: Case-2: Comparison of α_A response surfaces between gPC and ME-gPC for $U^* = 6.34$

Table 1: Mean and variance of α_A due to uncertainties in k_{α_1} and k_{α_3} by Monte Carlo simulations (MC) and a 3rd order adaptive multi-element generalized Polynomial Chaos (ME-gPC) expansion with $\theta_1 = 10^{-3}$, $\theta_2 = 0.5$ and $U^* = 6.34$

U^*	method	Cost (N_{MC} or N_{gPC})	$\bar{\alpha}_A$	$\sigma^2_{\alpha_A}$
6.34	MC	10^3	4.912	24.639
	MC	10^4	4.947	24.273
	MC	10^5	5.011	24.246
	MC	10^6	5.026	24.309
	MC	10^7	5.024	24.288
	gPC	432	5.024	24.285

agreement with Monte-Carlo simulations as reported in Table 1.

The successive steps in the refinement procedure of the stochastic grid are illustrated in Fig. 5 for the case $U^* = 6.34$. The cubature points of the stochastic grid for each element are represented using green symbols when the adaptivity criterion (Eq. 14) is satisfied. Otherwise, red symbols are used and the refinement process in the corresponding element is performed according to Eq. 16. Here, we have used $n_q = P + 1$ quadrature points along each random direction based on polynomial accuracy requirement.

We notice that elements are mainly refined around the region of low regularity of the solution (i.e. for $k_{\alpha_1} \approx 1.025$) as expected. Moreover, more refinement occurs along the k_{α_1} than the k_{α_3} direction, which makes sense considering the different sensitivities of the solution to these two parameters . Finally, Fig. 5d reveals that 8 grid-levels are required by ME-gPC to satisfy the imposed adaptivity criterion for all random sub-elements. The final total number of elements is $N = 15$ for this level of resolution and the corresponding number of cubature points or samples is $N_{gPC} = 432$. Here, N_{gPC} refers to the total number of deterministic runs required by the adaptive approach, including the runs generated at each intermediate step.

Next, the bifurcation diagram of the nonlinear stochastic aeroelastic model is explored by repeating the ME-gPC procedure for different non-dimensional velocities. Fig. 6 shows the response surfaces of α_A obtained for $U^* = [5.5, 6.23, 6.61, 7]$. The ME-gPC formulation is found to be very robust. Indeed, all types of response: purely deterministic (Fig. 6a), irregular (6b) and smooth response surfaces (Fig. 6b and Fig. 6c) are accurately captured using the same set of numerical parameters.

Getting to the physical analysis of the stochastic LCO, one can immediately observe from the pdf isocontours of α_A (Fig. 7) that the behaviour of the stochastic bifurcation can be divided into three distinct regions: a pre-bifurcation region characterized by a Dirac delta-type function at α_A=0 deg, meaning that damped oscillations are always obtained; a region for $U^* > 6$ that shows that it is possible to observe LCO; a post-bifurcation region for $U^* > 6.6$. In the second region, the value of $U^* = 6$ indicates that the flutter onset of the

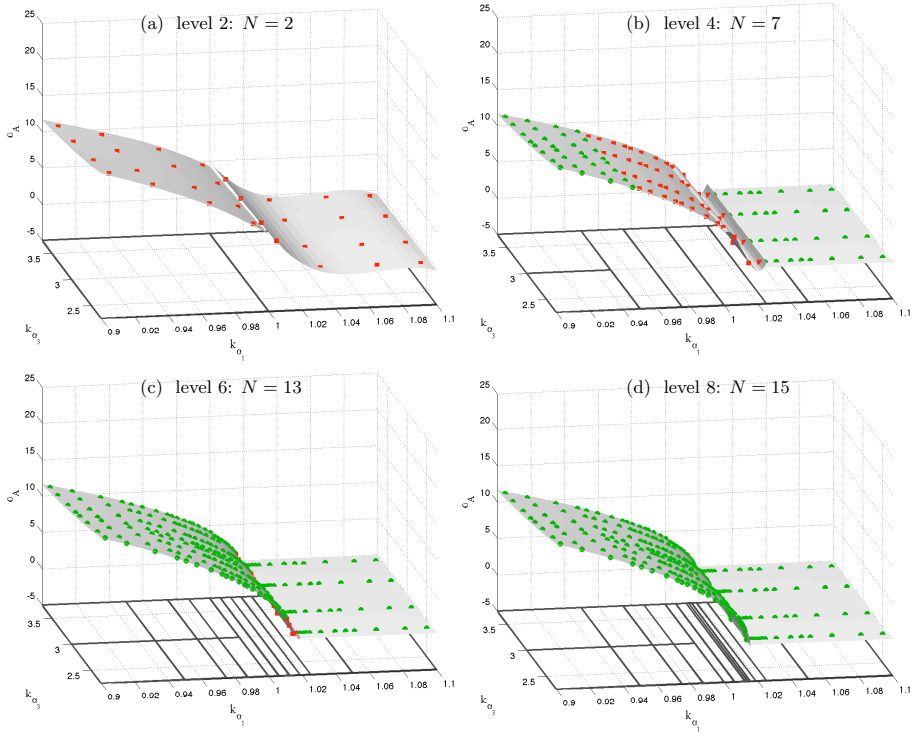

Figure 5: Case-2: Illustrative examples of the ME-gPC parametric grid-refinement process for the α_A response surface at $U^* = 6.34$ (red cubature points indicate that criterion of Eq. 14 is not satisfied in the random element of interest, and that refinement needs to be performed). Only intermediate levels of refinement are presented.

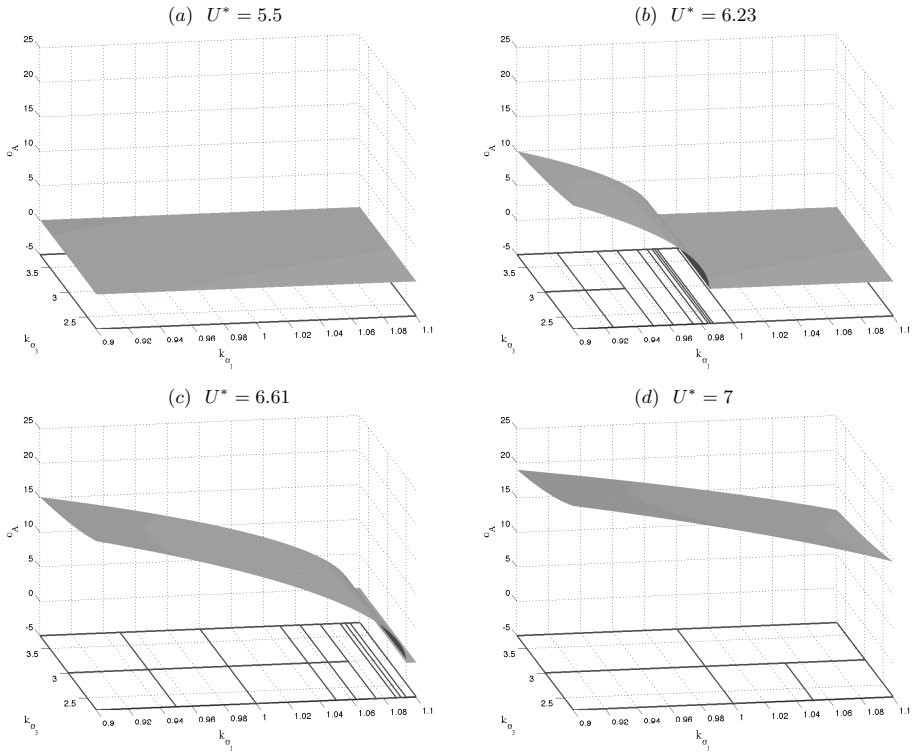

Figure 6: Examples of converged ME-gPC response surface obtained for different reduced velocities U^*.

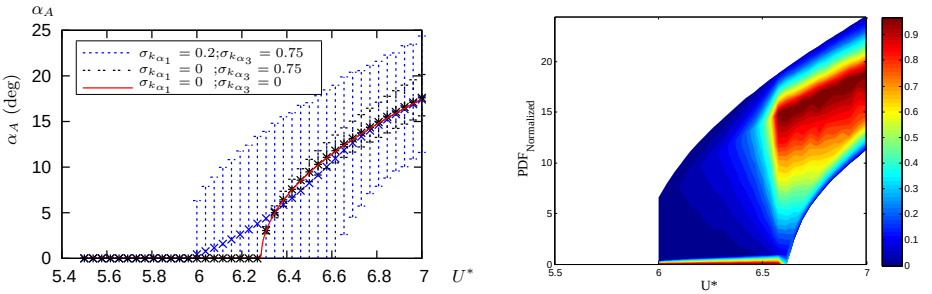

Figure 7: Case-2: ME-gPC pdf isocontours (right) and corresponding error bars (left) of α_A due to combined uncertainties in k_{α_1} and k_{α_3}

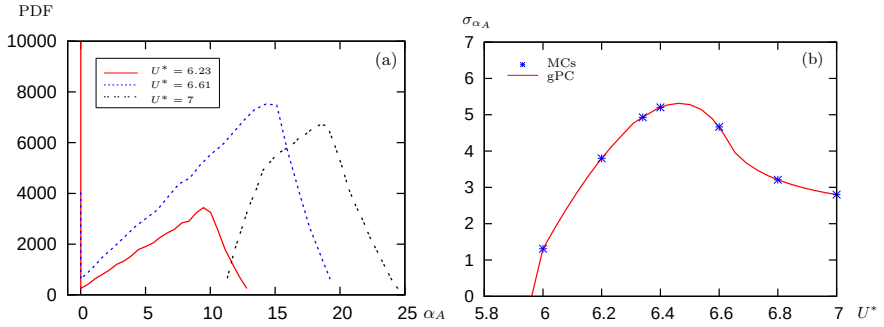

Figure 8: Case-2: (a) ME-gPC pdf of α_A profiles obtained with $P = 3$ for different reduced velocities and (b) comparison between ME-gPC and MC ($N_{MC} = 10^6$ samples) standard deviation results

stochastic simulations is approximatively 3.2% lower than that of the flutter speed obtained with deterministic k_{α_1}. The stochastic bifurcation is defined approximatively by $U^* \in [6, 6.6]$. Note that for $U^* \in [6.3, 6.7]$ the mean value $\bar{\alpha}_A$ is lower than $\bar{\alpha}_A$ obtained with only uncertain k_{α_3}. In the post-bifurcation region ($U^* > 6.6$) the mean values of α_A are similar for all simulations.

Typical plots of the pdf obtained in the bifurcation region ($U^* = 6.23$ and $U^* = 6.61$) are presented in Fig. 8a. One may notice on the shape of the pdf that both the Dirac delta-type function of the stationary branch and the local maximum due to the probability to capture stable LCO are visible. We also remark that the pdf obtained for the post-bifurcation regime (say $U^* = 7$ as shown in Fig. 8a) is not symmetric. This is the signature of the system nonlinearity.

Next, we look at the α_A solution variability depending on the reduced velocity. ME-gPC results are compared with MC results and show very good agreement for both stochastic bifurcation and post-bifurcation regimes (Fig. 8b). Quantitative comparison for $U^* = 7$ is reported in Table 2 where it has been verified that ME-gPC results are correctly converged. It is also interesting to note that the plots of the standard deviation of α_A against U^* strongly differs depending on the nature of the parametric uncertainties. Indeed, we have observed that $\sigma^2_{\alpha_A}$ growths linearly with U^* in the case of a single random parameter k_{α_3} (Fig. 2b). However, Fig. 8b shows that when a stochastic bifurcation is present (Case-2 with random k_{α_1} and k_{α_3}), the α_A std increases in the bifurcation region and reaches a maximum around $U^* = 6.5$ before to decrease when the stable LCO regime is established.

In terms of cost, the total number of cubature points N_{gPC} needed by the adaptive ME-gPC approach depending on the chosen polynomial order P is

Table 2: Mean and variance of α_A for $U^* = 7$ due to uncertainties in k_{α_1} and k_{α_3} by Monte Carlo simulations (MC) and a 3rd order adaptive ME-gPC expansion with $\theta_1 = 10^{-3}$, $\theta_2 = 0.5$.

U^*	method	Cost (N_{MC} or N_{gPC})	$\bar{\alpha}_A$	$\sigma^2_{\alpha_A}$
7	MC	10^3	17.476	7.513
	MC	10^4	17.420	7.749
	MC	10^5	17.419	7.818
	MC	10^6	17.418	7.839
	MC	10^7	17.421	7.845
	gPC	144	17.421	7.845

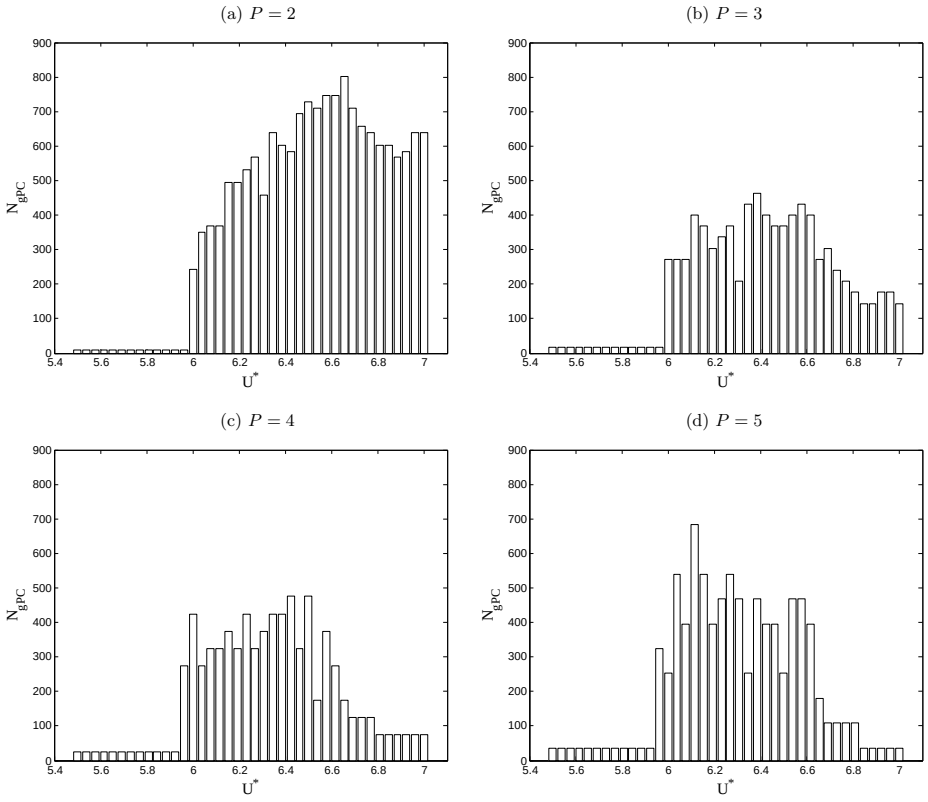

Figure 9: Case-2: Growth of the total number of ME-gPC elements cubature points N_{gPC} versus U^* and P.

plotted against the bifurcation parameters U^* in Fig. 9.

We notice that the number of samples is dictated by the sensitivity of the stochastic solution. Indeed, N_{gPC} increases in the stochastic bifurcation region until the probability of damped oscillations disappears completely ($U^* \approx 6.6$). Then, N_{gPC} decreases within the post bifurcation region.

Fig. 9a indicates that the method is more costly when $P = 2$ compared to computations based on $P \geq 3$. This is expected, based on the way the adaptive criteria operates, as using $P = 2$ means that mainly linear terms contribution will be retained in the reconstruction of a (possibly) non-linear response. Consequently, the use of $P = 3$ immediately reduces this drawback as shown in Fig. 9b. Note that the increase in P does not reduce significantly the number of samples N_{gPC} as far as irregular response surfaces are concerned (i.e in the stochastic bifurcation region). However, for smooth response (i.e. $U^* > 6.6$), the use of higher order gPC expansion consistently reduces the computational cost (9c and 9d). Keeping in mind that the number of cubature points per element is taken to be equal to $(P + 1)^d$, ME-gPC computations based on $P = 3$ (or $P = 4$) represent a good compromise between accuracy and associated computational cost.

The convergence properties of the ME-gPC formulation are now analysed by means of the convergence rates based on the variance of α_A. Fig. 10 shows results for uniformly refined meshes while Fig. 11 shows results for the ME-gPC with the adaptive refinement approach described in this paper.

Spectral $P-$convergence and algebraic $h-$convergence, with a convergence rate of $\mathrm{O}(N^{-N_q})$ where N_q is the number of Gauss quadrature points per direction, is obtained for the smooth response (with no discontinuity) corresponding to the post-bifurcation region (e.g. $U^* = 7$). Those results are in very good agreement with the theoretical rate estimates of Foo et al.[6] (represented here with short dashed lines). For the bifurcation state (e.g. $U^* = 6.34$), the convergence is poor and irregular on the uniform meshes with convergence rates stagnating around $\mathrm{O}(N^{-1})$. However, the approximation error is much lower for the adaptive approach and drops faster and sooner for larger mesh size and

U^*	$N^{(P=2)}/N^{(P=5)}$	$N_{gPC}^{(P=2)}/N_{gPC}^{(P=5)}$	ϵ
7.0	≈ 83	≈ 21	$\approx 2 \cdot 10^{-9}$
6.34	≈ 20	≈ 4	$\approx 9.5 \cdot 10^{-4}$

Table 3: Computational speedups of the adaptive ME-gPC approach – in terms of total number of elements and cubature points – due to the choice of the polynomial order of representation P for a given level of relative error in variance ϵ.

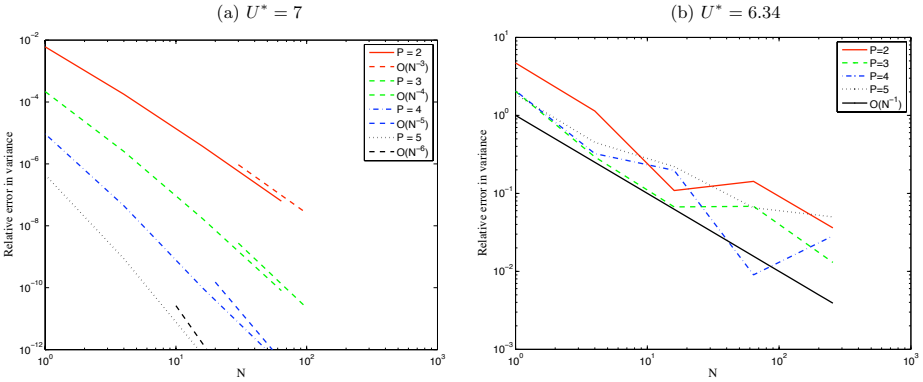

Figure 10: Case-2: h/p convergence rates of the non-adaptive ME-gPC variance of α_A for $U^* = 7.0$ (left) and $U^* = 6.34$ (right).

larger P (see Fig. 11-b). This results prove the superiority of the adaptive versus uniform refinement. Moreover, increasing the order of the polynomial allows some computational savings in terms of the total number of elements and the total number of runs (including intermediate stages). Table 3 shows that the adaptive computation is about 20 times faster for a choice of $P = 5$ than $P = 2$ for the smooth case $U^* = 7$ while it remains approximately 4 times faster for the bifurcation case $U^* = 6.34$ (cf. Fig. 11). Savings in terms of the total number of elements are even more substantial.

As a brief demonstration of the robustness of the method in capturing more complex response, we also present results obtained from combining randomness in the linear spring coefficient ($\bar{k}_{\alpha_1} = 1$, $\sigma_{k_{\alpha_1}} = 0.05$) and mass ratio ($\bar{\mu} = 100$, σ_μ=5). Me-gPC computations were performed using $P = 4$ and the threshold values used for the adaptive criteria are $\theta_1 = 5 \times 10^{-5}$ and $\theta_2 = 0.75$. As clearly visible in Fig. 12, the bifurcating front is not aligned with one of the parametric directions in this case. Instead, LCO are obtained at different k_{α_1} for varying mass ratio μ. We observe that the grid refinement adapts remarkably to the front although requiring more elements than the previous cases. The final number of elements after refinement is $N = 231$, which, in conjunction with of use of $P = 4$, corresponds to $N_{gPC} = 10525$ deterministic samples.

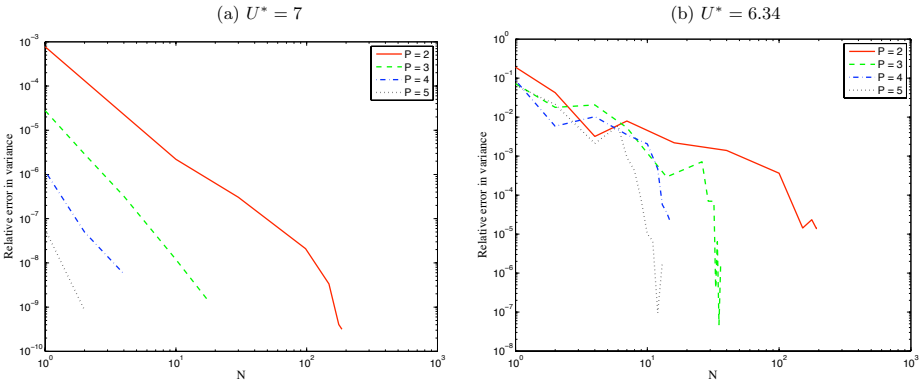

Figure 11: Case-2: h/p convergence rates of the adaptive ME-gPC variance of α_A for $U^* = 7.0$ (left) and $U^* = 6.34$ (right).

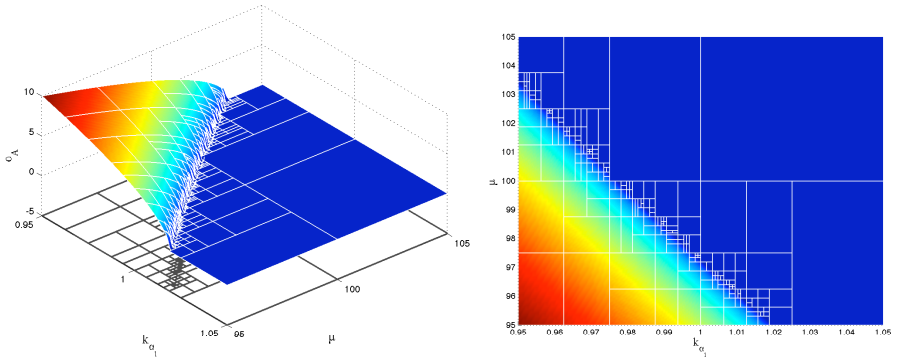

Figure 12: ME-gPC response surface due to uncertain k_{α_1} and μ obtained for $U^* = 6.2$ using $P = 4$ ($\bar{k}_{\alpha_1} = 1$, $\sigma_{k_{\alpha_1}} = 0.05$, $\bar{\mu} = 100$, $\sigma_\mu = 5$)

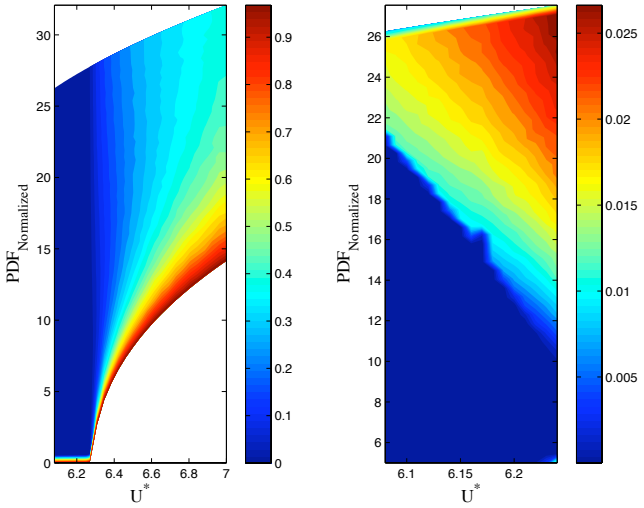

Figure 13: Case-3: ME-gPC pdf isocontours of α_A due to uncertain k_{α_3} with $\bar{k}_{\alpha_3} = 0$ and $\sigma_{k_{\alpha_3}} = 3.75$. The right plot shows a zoomed-in view of the pdf region of low reduced velocity ($k_{\alpha_1} = 1$, $k_{\alpha_5} = 20$, the colormap is adjusted).

4..3 *Case-3: Influence of wide span uncertainty in the cubic torsional stiffness term*

We now consider the sensitivity of the LCO peak to some randomness in k_{α_3}, while the *deterministic* value of the pentic pitch stiffness term is taken to be $k_{\alpha_5} = 20$ [24]. The novelty of the approach is that we now consider a wide span range of uncertainty for k_{α_3} that encompasses both negative (softening) and positive (hardening) spring values. The distribution is again chosen to be *uniform* and we pick the following range $k_{\alpha_3} \in [-3.75, 3.75]$. Notice that the non-zero probability associated with negative and positive values of k_{α_3} is likely to introduce several routes to instability (existence of supercritical vs. subcritical bifurcations) depending on the initial condition. It is therefore a more strenuous test for the numerical method.

We use an adaptive ME-gPC representation coupled with a deterministic Runge-Kutta time-integration ODE solver. A 3rd order Legendre Polynomial Chaos basis is used within each element and the refinement criteria is taken as $\theta_1 = 10^{-4}$. We chose an initial pitch angle $\alpha(0) = 12.5$ deg, while all other initial conditions ($\xi(0)$, $\alpha'(0)$,$\xi'(0)$) are set to zero. Cost is not an issue here and computations converge very quickly as there is only one uncertain parameter. Fig. 13 (left) shows the *normalized* pdf isocontours over the range : $U^* \in [6.08, 7]$ while the right plot shows a zoomed-in view of the pdf region defined by $U^* \in [6.08, 6.24]$. For $U^* > 6.3$, the pdf isocontours with non-zero values present a fan shape that gets wider with increasing U^*. This coincides with the capture of both the supercritical and subcritical branches that coalesce in one single region. Most probable solutions are always obtained for large positive values of k_{α_3} and correspond to small LCO oscillations. Least probable solutions are always obtained for large negative values of k_{α_3} and correspond to large LCO oscillations.

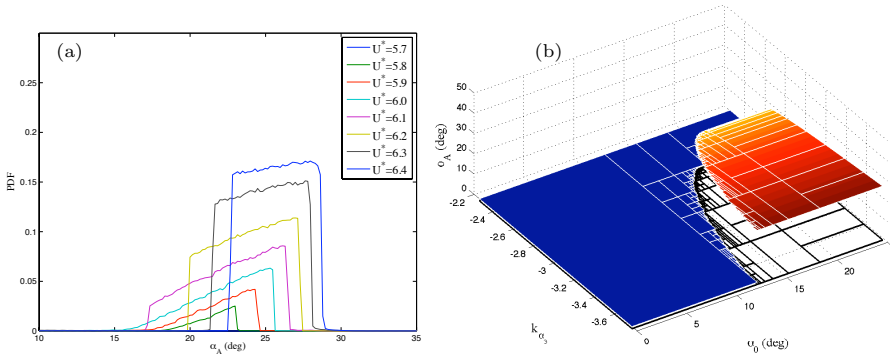

Figure 14: Case-4: (a) pdf of the stable large amplitude LCO branch for selected U^* and (b) corresponding ME-gPC response surface and grid vs. $\alpha(0)$ and k_{α_3} for $U^* = 6$

For $U^* < 6.3$ we observe a dominant Dirac delta function-like distribution for stable motion (i.e. $\alpha_A = 0$). This state corresponds to all $k_{\alpha_3} > 0$ realizations. For the $k_{\alpha_3} < 0$ range, and depending on the initial pitch value (here $\alpha(0) = 12.5$), there is a non-zero probability to get unstable motions capturing the LCO subcritical branch. Due to the low probability of occurrence, this region is masked on the left plot but appears clearly in the zoomed-in version (right plot). In this region, we notice that the most probable solutions are always obtained for large negative values of k_{α_3} and correspond to *large* LCO oscillations.
Therefore, we can conclude that there exists a particular range of reduced velocity, in which some rare events of large instabilities can take place for softening springs. This result emphasizes the importance of uncertainty quantification. Of course in this case, the choice of the initial condition remains of major importance.

4..4 *Case-4: subcritical stochastic bifurcation with random initial pitch angle and cubic spring term*

Finally, the sensitivity of the peak LCO to combined randomness in k_{α_3} and $\alpha(0)$ with *uniform* distribution is explored using ME-gPC coupled with the deterministic Runge-Kutta time-integration ODE solver. Other initial conditions $(\xi(0), \alpha'(0), \xi'(0))$ are set to zero.

The mean and the standard deviation of the input random parameters were taken as: $\bar{\alpha}(0) = 12.5$ deg, $\sigma_\alpha(0) = 12.5$ deg, $\bar{k}_{\alpha_3} = -3$ and $\sigma_{k_{\alpha_3}} = 0.75$. The bifurcation parameters were chosen as $U^* \in [5.7, 6.4]$.

Fig. 14a presents the α_A pdf of the stable large amplitude LCO branch computed using the adaptive ME-gPC solver. Each pdf is estimated from the ME-gPC expansions using $1M$ samples. We notice that the amplitude probability density functions depend strongly on the reduced velocity and that the response is more sensitive to the k_{α_3} parametric uncertainty. For reduced velocities above the bifurcation point ($U^* \geq 6.4$), the response results in unimodal density functions with distribution close to uniform. However, for reduced velocities in the range $U^* \in [5.8, 6.3]$, the density response is bimodal with an additional sharp Dirac delta-like peak (not represented here) corresponding to the zero-amplitude stable branch. This bimodal response results from the discontinuous shape of the response surface solution. For instance, one can see on Fig. 14b, the response surface computed for $U^* = 6$ which exhibits a discontinuous pattern where the boundary values of $\alpha(0)$ and k_{α_3} defining the jump from the stable branch to stable LCO is clearly visible.
Aside from this study with *uniformly* distributed inputs, one could wonder about the requirements and effects of changing the probability distributions of the random inputs. Another advantage of the gPC representation, as long as the surface fit is sufficiently accurate, is to be able to estimate the statistics of the response for different random input distributions, so long as the new input spans the

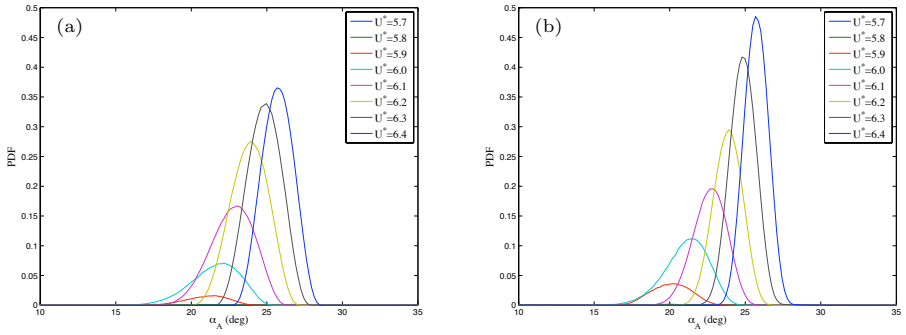

Figure 15: Case-4$^{(*)}$: pdf of the stable large amplitude LCO branch for selected U^* for $\alpha(0)$ and k_{α_3} following (a) $Beta(\alpha = 3, \beta = 3)$ distributions and (b) *uniform* $Beta(\alpha = 6, \beta = 6)$ distributions respectively

same domain of the probability space as the former. In this case, there is no need to recompute the response at new sample points and the new response statistics can be simply evaluated in a post-processing stage (directly from Eq. 8). In the following, we show results for Case-4 in which we change the type of parametric distributions while keeping the same parametric bounds for k_{α_3} and $\alpha(0)$ as in Case-4 (we refer to those cases as Case-4$^{(*)}$, see Fig. 15). We consider a case where both k_{α_3} and $\alpha(0)$ follow independent $Beta(\alpha = 3, \beta = 3)$ distributions (Fig. 15a) and another case where $\alpha(0)$ follows a *uniform* distribution and k_{α_3} a $Beta(\alpha = 6, \beta = 6)$ distribution (Fig. 15b). The obtained pdf shapes are very different from Case-4 but follow the same trend of getting narrower for higher U^* due to the change in the surface response plateau. Here, the distributions look similar to *Beta* distributions. However, careful examinations of the distribution tails indicate that there exists a bias for lower reduced velocities resulting in a longer left tail toward the zero-amplitude stable branch (Fig. 15a). This bias is reduced when $\alpha(0)$ follows a *uniform* distribution and the k_{α_3} *Beta* distribution is more narrow (Fig. 15b).

5. Conclusions

In this work, a non-intrusive $h-$adaptive stochastic solver, based on a Multi-Element generalized Polynomial Chaos expansions, along the lines of Foo et al.[6], was successfully employed to predict the LCO bifurcation diagram of an elastically mounted two-degree-of-freedom airfoil subject to random physical parameters and initial conditions. The random structural parameters were chosen to follow independent bounded distributed random variables and Legendre polynomials were used as the polynomial basis of representation within each sub-element. Full tensor product-based Gauss Legendre quadrature point sets were used in each element to evaluate the Galerkin projection of the approximated solution. Criteria of adaptivity for the parametric grid refinement was based on the local convergence of the solution variance.

The difficulty of this problem is due to the fact that LCO bifurcations for given reduced velocities translate in stochastic bifurcations or discontinuities of the solution against the parametric variability of the inputs. The adaptive methodology was able to track these fronts and provide accurate and converged solutions for both *uniform* and Beta random distributions. Results were validated against Monte-Carlo simulations. The robustness of the ME-gPC was demonstrated for several variety of stochastic configurations due to randomness in the torsional stiffness terms, mass ratio and initial pitch angle for a wide range of operating conditions.

In the case of the combined randomness in the linear and cubic spring coefficient, the solution bifurcation region was notably enlarged due to the randomness of the parameters. Probability density functions of the pitch angle have shown sudden change and variability from zero-amplitude stable branch to large LCO stable branch for a given reduced velocity. In the case of subcritical stochastic bifurcation with combined randomness in the initial pitch angle and

cubic spring coefficient with deterministic pentic spring coefficient, pitch angle probability density functions have shown the presence of a bimodal response with a strong variability of the probability of occurrence for the LCO stable branch.

References

[1] P.S. Beran, C.L. Pettit, and D.R. Millman. Uncertainty quantification of limit-cyle oscillations. *Journal of Computational Physics*, 217:217–247, 2006.

[2] M. Cai, J.K. Liu, and J. Li. Incremental harmonic balance method for airfoil flutter with multiple strong nonlinearities. *Applied Mathematics and Mechanics*, 27(7):953–958, 2006.

[3] R.H. Cameron and W.T. Martin. The orthogonal development of nonlinear functionals in series of fourier-hermite functionals. *Ann. Math.*, 48:385, 1947.

[4] J.-C. Chassaing and D. Lucor. Stochastic investigation of flows about airfoils at transonic speeds. *AIAA Journal*, 48(4), May 2010, DOI:10.2514/1.42637, 2010.

[5] E.H. Dowell, E.F. Crawley, H.C. Curtiss Jr, D.A Peters, R.H. Scanlan, and F. sisto. *A Modern Course in Aeroelasticity.* Kluwer academic publishers edition, 1995.

[6] J. Foo, X. Wan, and G.E. Karniadakis. The multi-element probabilistic collocation method (me-pcm): Error analysis and applications. *Journal of Computational Physics*, 227:9572–9595, 2008.

[7] Y.C. Fung. *An introduction to the theory of aeroelasticity.* Dover Publications, Inc., dover edition, 1993.

[8] R.G. Ghanem and P. Spanos. *Stochastic Finite Elements: a Spectral Approach.* Springer-Verlag, 1991.

[9] Gene H. Golub and John H. Welsch. Calculation of Gauss quadrature rules. *Math. Comp. 23 (1969)*, 23, 1969.

[10] S. Hosder, R.W. Walters, and R. Perez. A non-intrusive polynomial chaos method for uncertainty propagation in cfd simulations. AIAA Paper 2006–891, 2006.

[11] R.T Jones. The unsteady lift of a wing of finite aspect ratio. *NACA Report 681*, 1940.

[12] S.L. Lau and W.S. Zhang. Nonlinear vibrations of piecewise-linear systems by incremental harmonic balance method. *Journal of Applied Mechanics*, 59:153160, 1992.

[13] B.H.K. Lee, L.Y. Jiang, and Y.S. Wong. Flutter of an airfoil with cubic restoring force. *Journal of fluids and structures*, 13:75–101, 1999.

[14] B.H.K. Lee, L. Liu, and K.W. Chung. Airfoil motion in subsonic flow with strong cubic nonlinear restoring forces. *Journal of Sound and Vibration*, 281:699–717, 2005.

[15] B.H.K. Lee, S.J. Price, and Y.S. Wong. Nonlinear aeroelastic analysis of airfoils : bifurcation and chaos. *Progress in aerospace sciences*, 35:205–334, 1999.

[16] L. Librescu, G. Chiocchia, and P. Marzocca. Implications of cubic physical/aerodynamic non-linearities on the character of the flutter instability boundary. *International Journal of Non-Linear Mechanics*, 38:173–199, 2003.

[17] L. Liu and E.H. Dowell. Harmonic balance approach for an airfoil with a freeplay control surface. *AIAA Journal*, 43(4):802–815, 2005.

[18] L. Liu and E.H. Dowell. The secondary bifurcation of an aeroelastic airfoil motion: effect of high harmonics. *Nonlinear Dynamics*, 37:31–49, 2005.

[19] L. Liu and E.H. Dowell J.P. Thomas. A high dimensional harmonic balance approach for an aeroelastic airfoil with cubic restoring forces. *Journal of Fluids and Structures*, 23(3):351–363, 2007.

[20] L. Liu, J.P. Thomas, E.H. Dowell, P. Attar, and K.C. Hall. A comparison of classical and high dimensional harmonic balance approaches for a duffing oscillator. *Journal of Computational Physics*, 215(1):298–320, 2006.

[21] D. Lucor and G.E. Karniadakis. Noisy Inflows Cause a Shedding-Mode Switching in Flow past an Oscillating Cylinder. 92(15):154501–1; 154501–4, 2004.

[22] D. Lucor, J. Meyers, and P. Sagaut. Sensitivity analysis of LES to subgrid-scale-model parametric uncertainty using Polynomial Chaos. *Journal of Fluid Mechanics*, 585:255–279, 2007.

[23] D.R. Millman. Quantifying initial conditions and parametric uncertainties in a nonlinear aeroelastic system with an efficient stochastic algorithm. Technical report, PhD. Dissertation, Air Force Institute of Technology, september 2004.

[24] D.R. Millman, P.I. King, and P.S. Beran. Airfoil pitch-and-plunge bifurcation behavior with fourier chaos expansions. *Journal of Aircraft*, 42(2):376–384, 2005.

[25] C.L. Pettit. Uncertainty quantification in aeroelsticity: recent results and research challenges. *Journal of Aircraft*, 41(5):1217–1229, 2003.

[26] D.C. Poirel and S.J. Price. Structurally nonlinear fluttering airfoil in turbulent flow. *AIAA Journal*, 39(10):1960–1968, 2001.

[27] D.C. Poirel and S.J. Price. Bifurcation characteristics of a two-dimensional structurally non-linear airfoil in turbulent flow. *Nonlinear Dynamics*, 48:423–435, 2007.

[28] G. Poëtte, B. Després, and D. Lucor. Uncertainty quantification for systems of conservation laws. *Journal of Computational Physics*, 228:2443–2467, 2009.

[29] W. Schoutens. *Stochastic processes in the Askey scheme*. PhD thesis, K.U. Leuven, 1999.

[30] S.A. Smolyak. Quadrature and interpolation formulas for tensor products of certain classes of functions. *Soviet Mathematics, Doklady*, 4:240–243, 1963.

[31] Lloyd N. Trefethen. Is gauss quadrature better than clenshaw-curtis? *SIAM Rev.*, 50(1):67–87, 2008.

[32] R.W. Walters. Towards stochastic fluid mechanics via polynomial chaos. AIAA Paper 2003–413, 2003.

[33] X. Wan and G.E. Karniadakis. An adaptive multi-element generalized polynomial chaos method for stochastic differential equations. *Journal of Computational Physics*, 209:617–642, 2005.

[34] X. Wan and G.E. Karniadakis. Multi-element generalized polynomial chaos for arbitrary probability measures. *SIAM Journal of Scientific Computing*, 28(3):901–928, 2006.

[35] X. Wan and G.E. Karniadakis. Stochastic heat transfer enhancement in a grooved channel. *Journal of Fluid Mechanics*, 565:255–278, 2006.

[36] J.A.S. Witteveen and H. Bijl. An alternative unsteady adaptive stochastic finite elements formulation based on interpolation at constant phase. *Computer Methods in Applied Mechanics and Engineering*, 198(3-4):578–591, 2008.

[37] J.A.S. Witteveen and H. Bijl. An unsteady adaptative stochastic finite elements formulation for rigid-body fluid-structure interaction. *Computers and Structures*, 86:2123–2140, 2008.

[38] J.A.S. Witteveen and H. Bijl. Higher period stochastic bifurcation of nonlinear airfoil fluid-structure interaction. *Math. Probl. Eng.*, 2009. In Press.

[39] J.A.S. Witteveen and H. Bijl. A tvd uncertainty quantification method with bounded error applied to transonic airfoil flutter. *Communications in Computational Physics*, 6:406–432, 2009.

[40] J.A.S. Witteveen, A. Loeven, S. Sarkar, and H. Bijl. Probabilistic collocation for period-1 limit cycle oscillations. *Journal of Sound and Vibration*, 311(311):421–439, 2008.

[41] C. Wu, H. Zhang, and T. Fang. Flutter analysis of an airfoil with bounded random parameters in compressible flows via gegenbauer polynomial approximation. *Aerospace Science and Technology*, 11:518–526, 2007.

[42] D. Xiu and G.E. Karniadakis. Modeling uncertainty in flow simulations via generalized polynomial chaos. *J. Comput. Phys.*, 187:137–167, 2003.